REPORT DOCUMENTATION PAGE

AFRL-SR-BL-TR-02-

0155

1. AGENCY USE ONLY *(Leave blank)*	2. REPORT DATE	3. RI
	28 MAR 02	FINAL (01 JAN 01 TO 31 AUG 01

4. TITLE AND SUBTITLE
ACTIVE AEROELASTIC TAILORING OF HIGH-ASPECT-RATIO COMPOSITES WINGS

5. FUNDING NUMBERS
F49620-01-1-0133

6. AUTHOR(S)
CARLOS CESNIK

7. PERFORMING ORGANIZATION NAME(S) AND ADDRESS(ES)
MIT ROOM 33-316
77 MASSACHUSETTS AVENUE
CAMBRIDGE, MA 02139-4307

8. PERFORMING ORGANIZATION REPORT NUMBER

9. SPONSORING/MONITORING AGENCY NAME(S) AND ADDRESS(ES)
AFOSR
801 N. RANDOLPH STREET
ARLINGTON, VA 22203

10. SPONSORING/MONITORING AGENCY REPORT NUMBER

11. SUPPLEMENTARY NOTES

12a. DISTRIBUTION AVAILABILITY STATEMENT

Approved for public release; distribution unlimited.

12b. DISTRIBUTION CODE

13. ABSTRACT *(Maximum 200 words)*
The objective of the proposed work is to study the fundamental mechanisms of active aeroelastic tailoring of high-aspect-ratio composite wings. The emphasis will be on actively exploring structural flexibility to enhance flight performance and reduce structural weight, while controlling aeroelastic instabilities. To investigate the effects of distributed anisotropic strain actuation and their synergism with the passive aeroelastic tailored composite structure, a suitable nonlinear active aeroelastic framework is required. Therefore, an analysis and design tool is being developed for high aspect ratio active flexible wings. The formulation is capable of modeling the nonlinear large deflection behavior of the wings, deformation due to applied voltages on the active plies in the skin of the wing, and the unsteady subsonic aerodynamic forces acting on the wing. Because the wing is ling and slender, it can be reasonably well modeled as a beam undergoing three dimensional displacements and rotations. The cross sectional stiffness, inertia, and actuation properties of the wing are calculated along the span, and then a 1-d nonlinear beam model is constructed. This is a novel beam representation that is based on the beam curvatures, resulting in a computationally efficient low-order model suitable for preliminary structural design and control synthesis. Preliminary numerical results are presented in this report.

14. SUBJECT TERMS

15. NUMBER OF PAGES
10

16. PRICE CODE

17. SECURITY CLASSIFICATION OF REPORT	18. SECURITY CLASSIFICATION OF THIS PAGE	19. SECURITY CLASSIFICATION OF ABSTRACT	20. LIMITATION OF ABSTRACT
UNCLASSIFIED	UNCLASSIFIED	UNCLASSIFIED	

PROGRESS REPORT
January–August 2001

GRANT NUMBER F49620-01-1-0133

ACTIVE AEROELASTIC TAILORING OF HIGH-ASPECT-RATIO COMPOSITE WINGS

Principal Investigator:
Carlos E. S. Cesnik
Associate Professor of Aeronautics and Astronautics
Massachusetts Institute of Technology
77 Massachusetts Avenue 33-316
Cambridge, Massachusetts 02139

Program Manager:
Dr. Daniel Segalman
AFOSR/NA
Program Manager, Structural Mechanics
801 N. Randolph Street Room 942
Arlington, Virginia 22203-1997
Telephone: (703) 696-7259
Fax: (703) 696-8451

Abstract

The objective of the proposed work is to study the fundamental mechanisms of active aeroelastic tailoring of high-aspect-ratio composite wings. The emphasis will be on actively exploring structural flexibility to enhance flight performance and reduce structural weight, while controlling aeroelastic instabilities. To investigate the effects of distributed anisotropic strain actuation and their synergism with the passive aeroelastic tailored composite structure, a suitable nonlinear active aeroelastic framework is required. Therefore, an analysis and design tool is being developed for high aspect ratio active flexible wings. The formulation is capable of modeling the nonlinear large deflection behavior of the wings, deformation due to applied voltages on the active plies in the skin of the wing, and the unsteady subsonic aerodynamic forces acting on the wing. Because the wing is long and slender, it can be reasonably well modeled as a beam undergoing three dimensional displacements and rotations. The cross sectional stiffness, inertia, and actuation properties of the wing are calculated along the span, and then a 1-D nonlinear beam model is constructed. This is a novel beam representation that is based entirely on the beam curvatures, resulting in a computationally efficient low-order model suitable for preliminary structural design and control synthesis. Preliminary numerical results are presented in this report.

ACTIVE AEROELASTIC TAILORING OF HIGH ASPECT RATIO COMPOSITE WINGS

Abstract

The objective of the proposed work is to study the fundamental mechanisms of active aeroelastic tailoring of high-aspect-ratio composite wings. The emphasis will be on actively exploring structural flexibility to enhance flight performance and reduce structural weight, while controlling aeroelastic instabilities. To investigate the effects of distributed anisotropic strain actuation and their synergism with the passive aeroelastic tailored composite structure, a suitable nonlinear active aeroelastic framework is required. Therefore, an analysis and design tool is being developed for high aspect ratio active flexible wings. The formulation is capable of modeling the nonlinear large deflection behavior of the wings, deformation due to applied voltages on the active plies in the skin of the wing, and the unsteady subsonic aerodynamic forces acting on the wing. Because the wing is long and slender, it can be reasonably well modeled as a beam undergoing three dimensional displacements and rotations. The cross sectional stiffness, inertia, and actuation properties of the wing are calculated along the span, and then a 1-D nonlinear beam model is constructed. This is a novel beam representation that is based entirely on the beam curvatures, resulting in a computationally efficient low-order model suitable for preliminary structural design and control synthesis. Preliminary numerical results are presented in this report.

Status of Effort

During these first eight months of this study, considerable progress was made towards the development of the active-flexible-wing analysis formulation. This is a fundamental component for the investigation of the effects of embedded anisotropic actuation on the aeroelastic response of high-aspect-ratio composite wings. Moreover, it was found that the nonlinear beam problem can be represented solely by tracking beam curvatures in a very natural way without ever having to introduce displacement or rotation variables. These can be later recovered by appropriate relations between them and the determined curvatures. Preliminary validation of the formulation has been conducted, and further numerical studies are expected for this next phase of the program.

Introduction

In the design of aircraft wings, the goal is usually to minimize the weight of the wings for a given payload weight. In the optimal design process, the structure of the wings is reduced until design constraints become active. Reducing the weight of the structure tends to produce wings that are more flexible, resulting in a lower flutter speed. At the optimal design point, it is possible that one or even all the constraints associated with flutter, divergence, and strength be active. Furthermore, flexible wings will undergo large deflections, making their aeroelastic response more complex to analyze and control using linear analysis tools and control methods. However, replacing the conventional flaps and ailerons with conformable surfaces with embedded anisotropic piezoelectric materials in the skin may lead to lighter designs. Two are the main reasons for that:

1. The actuatuors are integral to the structure, and contribute to its overall stiffness; it eliminates the extra weight associated with hydraulic lines and mechanical linkages.

2. The active wings will be able to extend the flutter and divergence boundaries through active control, allowing for a new optimal design point to be reached.

In the structural design of active flexible wings, a daunting amount of trade studies must take place in order to realize the best active/passive layup on the skin. The following observations apply:

1. In order to achieve the desired deformation, the stiffness of the active plies must be a significant fraction of the overall stiffness of the wings.

2. Active ply orientations that produce high twist authority may exhibit other negative qualities, such as greater static deflections and higher stresses in the passive plies.

3. The behavior of the wings may depend highly on the aeroelastic steady state at the given flight condition.

To navigate such a rich structural design space, where the aeroelastic behavior is not well known requires a priori understanding of the fundamental effects involved in the problem and potentially large degree of iteration. The current phase of this study concentrates on the development of a numerical procedure for determining the best active-passive layup, sensor locations, and controller architecture, which satisfy the lift and roll maneuver requirements over the operating flight envelope. The derivation of the equations of motion for the two-wing active roll model will be briefly discussed in this report. Work on the controller/structure automated design scheme will follow.

Model Formulation

The formulation of the equations of motion governing the roll and flexible wing motion are derived using the principle of virtual work. The high aspect ratio wings are modeled as three-dimensional beams, which can undergo large deflections. It is required to know the stiffness, mass, and inertia distributions as function of wing span. The formulation of the equations of motion for the wing consists of an analysis over the cross section based on the work of [3]. There, the active and passive layup and airfoil shape yield a set of actuation, stiffness and inertia properties for the cross section. For a tapered wing, the cross sectional analysis must be performed at several stations along the span, such that the properties can be interpolated. The result is a one-dimensional curvilinear reference line with a distribution of bending and twisting stiffness, mass and inertia, and center of gravity offsets. The location of the beam reference line can be arbitrarily placed at a percentage of chord, or can be placed at the computed elastic axis or area centroid. The curvature-based beam structural representation is very efficient and appropriate for the aeroelastic formulation being pursued. To the best knowledge of the PI, this is a new way of representing the linear and nonlinear beam dynamics problem.

Kinematics

Let $U^b = [\underline{u}_X, \underline{u}_Y, \underline{u}_Z]$ represent the body reference frame. The positions of the points at the root of the right and left wings are fixed in the body frame and are given by $\underline{P}^r(0)$ and $\underline{P}^l(0)$, corresponding to the wing curvilinear coordinate s=0. The direction vector $\underline{u}_x^r(s)$ points along the right wing reference axis. $\underline{u}_y^r(s)$ points toward the tip chord, and $\underline{u}_z^r(s)$ points in the airfoil z-direction. The left wing is similarly defined. Then, assuming that the wing reference axis remains of constant length, and that shearing deformation has negligible effect on the kinematics of deformation, the positions and direction vectors as a function of the curvilinear coordinate, s, are

$$\begin{aligned}
\frac{d}{ds}\underline{P}(s) &= \underline{u}_x(s) \\
\frac{d}{ds}\underline{u}_x(s) &= -\kappa_y(s)\underline{u}_z(s) + \kappa_z(s)\underline{u}_y(s) \\
\frac{d}{ds}\underline{u}_y(s) &= \kappa_x(s)\underline{u}_z(s) - \kappa_z(s)\underline{u}_x(s) \\
\frac{d}{ds}\underline{u}_z(s) &= -\kappa_x(s)\underline{u}_y(s) + \kappa_y(s)\underline{u}_x(s)
\end{aligned} \tag{1}$$

where $\kappa_x(s), \kappa_y(s)$, and $\kappa_z(s)$ represent the twisting, flat-wise bending, and chord-wise bending curvatures, respectively. The position and direction vectors along the span are given by

$$\begin{aligned}
\underline{P}(s) = \underline{P}^0 + \int_0^s \underline{u}_x(\varsigma)d\varsigma &= \underline{P}^0 + \int_0^s \left(\underline{u}_x^0 + \int_0^s \left(-\kappa_y(\varsigma)\underline{u}_z(\varsigma) + \kappa_y(\varsigma)\underline{u}_z(\varsigma)\right)d\varsigma \right) d\varsigma \\
\underline{u}_x(s) &= \underline{u}_x^0 + \int_0^s \left(-\kappa_y(\varsigma)\underline{u}_z(\varsigma) + \kappa_y(\varsigma)\underline{u}_z(\varsigma)\right)d\varsigma \\
\underline{u}_x(s) &= \underline{u}_x^0 + \int_0^s \left(\kappa_x(\varsigma)\underline{u}_y(\varsigma) - \kappa_z(\varsigma)\underline{u}_x(\varsigma)\right)d\varsigma \\
\underline{u}_x(s) &= \underline{u}_x^0 + \int_0^s \left(-\kappa_x(\varsigma)\underline{u}_y(\varsigma) + \kappa_y(\varsigma)\underline{u}_x(\varsigma)\right)d\varsigma
\end{aligned} \tag{2}$$

Given the position and direction vectors at the root, and the distribution of curvature along s, the shape of the wing is completely defined through equation 2. The wing is discretized at nk equally spaced points at the coordinates $\underline{s}_k$, between which the curvatures are linearly interpolated.

Inertial Elastic and Piezoelectric Forces and Moments

The internal elastic and piezoelectric forces and moments acting on a point on the reference line are given by

$$\begin{bmatrix} F_1 \\ M_1 \\ M_2 \\ M_3 \end{bmatrix} = \begin{bmatrix} B_{11} & B_{12} & \cdots & B_{1,m} \\ B_{21} & B_{22} & \cdots & B_{2,m} \\ B_{31} & B_{32} & \cdots & B_{3,m} \\ B_{41} & B_{42} & \cdots & B_{4,m} \end{bmatrix} \begin{bmatrix} V_1 \\ V_2 \\ \vdots \\ V_m \end{bmatrix} - \begin{bmatrix} K_{11} & K_{12} & K_{13} & K_{14} \\ K_{21} & K_{22} & K_{23} & K_{24} \\ K_{31} & K_{32} & K_{33} & K_{34} \\ K_{41} & K_{42} & K_{43} & K_{44} \end{bmatrix} \begin{bmatrix} \varepsilon_1 \\ \kappa_1 \\ \kappa_2 \\ \kappa_3 \end{bmatrix} \tag{3}$$

where the coefficient matrices are found by the cross sectional analysis of [3]. The 4 x 4 stiffness matrix in this derivation is a reduced form of 6 x 6 matrix, in which the transverse shear strains have been condensed out, but not neglected. The formulation of [3] accounts for the effects of anisotropic piezoelectric strain actuation in the active composite plies. In the present implementation, the derivation of [3] has been modified to facilitate the inclusion into a global optimization scheme, whereby the active and passive layup material constants, thicknesses, ply angles, and geometry are treated as variables. The number of applied voltages in equation (3) is equal to the number of active plies in the cross section, and will be determined in the (semi) automated design process. The minor changes to the implementation include the data format for specifying the cross section geometry, and the method in which path integrals are carried out. The present implementation was verified successfully against results of [3].

During the cross-section calculations, a set of recovery matrices are constructed which relate the 1-D beam strains and applied voltages to the distribution of strain and stress in each ply of the cross section. These values will be an important driving force in the design optimization to influence changes in the cross section variables. The ply strains are recovered at finely discretized points on the cross section contour and the ply stresses are determined based on the plane stress relation,

$$\begin{bmatrix} \sigma_1 \\ \sigma_2 \\ \sigma_3 \end{bmatrix} = \begin{bmatrix} Q_{11} & Q_{12} & 0 \\ Q_{21} & Q_{22} & 0 \\ 0 & 0 & Q_{66} \end{bmatrix} \left(\begin{bmatrix} \varepsilon_1 \\ \varepsilon_2 \\ \varepsilon_3 \end{bmatrix} - \begin{bmatrix} d_{11} \\ d_{12} \\ 0 \end{bmatrix} \frac{V}{t} \right) \tag{4}$$

where the free strain due to actuation is taken into account in the active plies. The present implementation allows for the inclusion of an internal web which may be active.

Inertial Forces and Moments

The inertial forces and moments acting at the center of gravity of the cross section must be referred to the beam reference line. The acceleration of the center of gravity of the cross section is given by $\bar{a}_{cg} = \bar{a}_{ra} + \bar{r}_{cg} \times \dot{\bar{\omega}}$, where the subscripts *cg* and *ra* correspond to the center of gravity and reference axis, respectively.
Then the forces and moments per unit length acting on the reference line are related to the reference line accelerations by the matrix relationship

$$\begin{bmatrix} F_x(s) \\ F_y(s) \\ F_z(s) \\ M_x(s) \\ M_y(s) \\ M_z(s) \end{bmatrix} = -\left[\begin{array}{ccc|ccc} \rho & 0 & 0 & 0 & \rho r_z & -\rho r_y \\ 0 & \rho & 0 & -\rho r_z & 0 & \rho r_x \\ 0 & 0 & \rho & \rho r_y & -\rho r_x & 0 \\ \hline 0 & -\rho r_z & \rho r_y & I_{xx} + \rho(r_y^2 + r_z^2) & I_{xy} - \rho r_x r_y & I_{xz} - \rho r_x r_z \\ \rho r_z & 0 & -\rho r_x & I_{yx} - \rho r_x r_y & I_{yy} + \rho(r_x^2 + r_z^2) & I_{yz} - \rho r_y r_z \\ -\rho r_y & \rho r_x & 0 & I_{zx} - \rho r_x r_z & I_{zy} - \rho r_y r_z & I_{zz} + \rho(r_y^2 + r_y^2) \end{array}\right] \begin{bmatrix} \ddot{x}(s) \\ \ddot{y}(s) \\ \ddot{z}(s) \\ \ddot{\theta}_x(s) \\ \ddot{\theta}_y(s) \\ \ddot{\theta}_z(s) \end{bmatrix} \tag{5}$$

where the forces and accelerations are resolved in the local frame of the deformed reference line. A vector quantity can be converted from the local to body frames by the rotation matrix $f^b = C^{ba} f^a$. It is more convenient, however, to construct the matrix that converts all of the nodal force vectors from the local to the body frame at once. Then a vector of $3np$ x 1 nodal forces is converted from the set of np local frames to the body frame by the relation $\underline{F}^b = U_a^b \underline{F}^a$, where U_a^b is a 3 np x $3np$ rotation matrix.

Equations of Motion

To apply the Principle of Virtual Work, the virtual work done by all internal and external forces must be expressed in terms of the set of independent generalized variables. The internal forces include elastic and actuation forces acting on the reference line. The external forces are all referred to the reference line and include gravity, inertial, and aerodynamic forces. The total work done by these forces can be divided into three parts,

1. The virtual work done on the right wing:

$$\delta W_1 = \int_{\text{right wing}} \left\{ \delta \underline{\varepsilon}' (\underline{F}^{(a)} - [K]\underline{\varepsilon}) + \delta \underline{P}' (\underline{F}^{dst} - [\rho]\ddot{\underline{P}} - [\rho r]\ddot{\underline{\theta}}) + \delta \underline{\theta}' (\underline{M}^{dst} + [\rho r]\ddot{\underline{P}} - [I]\ddot{\underline{\theta}}) \right\} ds \tag{6}$$

2. The virtual work done on the left wing:

$$\delta W_2 = \int_{\text{left wing}} \left\{ \delta \underline{\varepsilon}' (\underline{F}^{(a)} - [K]\underline{\varepsilon}) + \delta \underline{P}' (\underline{F}^{dst} - [\rho]\ddot{\underline{P}} - [\rho r]\ddot{\underline{\theta}}) + \delta \underline{\theta}' (\underline{M}^{dst} + [\rho r]\ddot{\underline{P}} - [I]\ddot{\underline{\theta}}) \right\} ds \tag{7}$$

3. The work done against the fuselage inertia (roll only)

$$\delta W_3 = \delta\phi I_f \ddot{\phi} \tag{8}$$

where ϕ is the roll angle, and I_f is the inertia of the fuselage. The local accelerations are related to the generalized accelerations through the Jacobian matrix relationship,

$$\ddot{\underline{P}}_{local} = [U_a^b]\ddot{\underline{P}}_{body} = [U_a^b]\left([J_{11}]\ddot{\underline{\kappa}} + [J_{12}]\ddot{\phi} \right) \tag{9}$$

Discretization and Numerical Itegration

The curvature variables are discretized at *nk* equally spaced points along the wing, at the coordinates, $\underline{s}_k$. The displacements, rotations, and forces and moments are discretized at *np* equally spaced points along the wing, at the coordinates, $\underline{s}_p$. Since a linear distribution of curvature cannot be represented by a linear distribution of distplacements, the displacement discretization is chosen to be finer than the curvature discretization.

A vector of forces defined at the coordinates $\underline{s}_p$ can be interpolated to the coordinates $\underline{s}_f$ by the matrix relation $\underline{s}_f = [ap]\underline{s}_p$. The coordinates $\underline{s}_f$ are of fine spacing suitable for numerical integration. The integral equations describing virtual work can be written as matrix relations by using interpolation matrices and inner products. In matrix form, the total virtual work relations becomes

1. Right wing

$$\delta W_1 = \delta \underline{\varepsilon}' \left([B_v]\underline{v} - [K]\underline{\varepsilon} \right) + \delta \underline{p}' \left([B_f]\underline{F}^{dst} + \underline{F}^{pt} - [M_{11}]\ddot{\underline{p}} - [M_{12}]\ddot{\underline{\theta}} \right) + \delta \underline{\theta}' \left([B_m]\underline{M}^{dst} + \underline{M}^{pt} - [M_{21}]\ddot{\underline{p}} - [M_{22}]\ddot{\underline{\theta}} \right)$$

2. Left wing

$$\delta W_2 = \delta \underline{\varepsilon}' \left([B_v]\underline{v} - [K]\underline{\varepsilon} \right) + \delta \underline{p}' \left([B_f]\underline{F}^{dst} + \underline{F}^{pt} - [M_{11}]\ddot{\underline{p}} - [M_{12}]\ddot{\underline{\theta}} \right) + \delta \underline{\theta}' \left([B_m]\underline{M}^{dst} + \underline{M}^{pt} - [M_{21}]\ddot{\underline{p}} - [M_{22}]\ddot{\underline{\theta}} \right)$$

where,

$$\underline{\varepsilon} = \begin{bmatrix} \underline{\varepsilon}_x \\ \underline{\kappa}_x \\ \underline{\kappa}_y \\ \underline{\kappa}_z \end{bmatrix}, \quad \underline{p} = \begin{bmatrix} \underline{x} \\ \underline{y} \\ \underline{z} \end{bmatrix}, \quad \underline{\theta} = \begin{bmatrix} \underline{\theta}_x \\ \underline{\theta}_y \\ \underline{\theta}_z \end{bmatrix}, \quad \underline{F}^{dst} = \begin{bmatrix} \underline{F}_x^{dst} \\ \underline{F}_y^{dst} \\ \underline{F}_z^{dst} \end{bmatrix}, \quad \underline{M}^{dst} = \begin{bmatrix} \underline{M}_x^{dst} \\ \underline{M}_y^{dst} \\ \underline{M}_z^{dst} \end{bmatrix}, \quad \underline{F}^{pt} = \begin{bmatrix} \underline{F}_x^{pt} \\ \underline{F}_y^{pt} \\ \underline{F}_z^{pt} \end{bmatrix}, \quad \underline{M}^{pt} = \begin{bmatrix} \underline{M}_x^{pt} \\ \underline{M}_y^{pt} \\ \underline{M}_z^{pt} \end{bmatrix}, \quad \underline{v} = \begin{bmatrix} \underline{v}_1 \\ \underline{v}_2 \\ \vdots \\ \underline{v}_m \end{bmatrix}$$

Application of the PVW yields the second order matrix equilibrium equations of motion, which includes the flexible motion, roll motion input at the wing root, and applied voltages, forces, and moments.

$$\left[\begin{array}{c|c|c} M_{11} & 0 & M_{13} \\ \hline 0 & M_{22} & M_{23} \\ \hline M_{31} & M_{32} & M_{33} \end{array}\right] \begin{bmatrix} \ddot{\underline{\kappa}}_r \\ \ddot{\underline{\kappa}}_l \\ \ddot{\phi} \end{bmatrix} + \left[\begin{array}{c|c|c} C_{11} & 0 & C_{13} \\ \hline 0 & C_{22} & C_{23} \\ \hline C_{31} & C_{32} & C_{33} \end{array}\right] \begin{bmatrix} \dot{\underline{\kappa}}_r \\ \dot{\underline{\kappa}}_l \\ \dot{\phi} \end{bmatrix} + \left[\begin{array}{c|c|c} K_{11} & 0 & 0 \\ \hline 0 & K_{22} & 0 \\ \hline 0 & 0 & 0 \end{array}\right] \begin{bmatrix} \underline{\kappa}_r \\ \underline{\kappa}_l \\ \phi \end{bmatrix} = \begin{bmatrix} \underline{F}_1 \\ \underline{F}_2 \\ \underline{F}_3 \end{bmatrix}$$

$$\begin{bmatrix} \underline{F}_1 \\ \underline{F}_2 \\ \underline{F}_3 \end{bmatrix} = \begin{bmatrix} B_{11} & 0 \\ 0 & B_{22} \\ 0 & 0 \end{bmatrix} \begin{bmatrix} \underline{v}_r \\ \underline{v}_l \end{bmatrix} + \begin{bmatrix} B_{13} & 0 \\ 0 & B_{24} \\ 0 & 0 \end{bmatrix} \begin{bmatrix} \underline{F}_r^{dst} \\ \underline{F}_l^{dst} \end{bmatrix} + \begin{bmatrix} B_{15} & 0 \\ 0 & B_{26} \\ 0 & 0 \end{bmatrix} \begin{bmatrix} \underline{M}_r^{dst} \\ \underline{M}_l^{dst} \end{bmatrix} + \begin{bmatrix} B_{17} & 0 \\ 0 & B_{28} \\ 0 & 0 \end{bmatrix} \begin{bmatrix} \underline{F}_r^{pt} \\ \underline{F}_l^{pt} \end{bmatrix} + \begin{bmatrix} B_{29} & 0 \\ 0 & B_{2,10} \\ 0 & 0 \end{bmatrix} \begin{bmatrix} \underline{M}_r^{pt} \\ \underline{M}_l^{pt} \end{bmatrix}$$

The aerodynamic and gravity forces and moments expressed in the input vectors on the right hand side must be expressed in terms of the generalized variables to produce an effective state-space model of the system.

Unsteady Aerodynamics Model

The unsteady aerodynamic forces and moments are computed using the approach of [5], which calculates the unsteady loads on a deformable airfoil in subsonic flow. The aerodynamic loads can be represented in terms of the well-known pitch and plunge variables, as well as the induced flow due to free vorticity. The method allows for the aerodynamic loads to be efficiently incorporated into the state space representation, and requires induced flow states to be added to the structural states. By relating the pitch and plunge motion to the generalized variables, the aerodynamic forces can be written in matrix form as

$$\underline{F}_r^{aero} = G_{11}\ddot{\underline{\kappa}}_r + G_{13}\ddot{\phi} + G_{14}\dot{\underline{\kappa}}_r + G_{16}\dot{\phi} + G_{110}\underline{\lambda}_r + G_{112}\underline{\alpha}_r$$
$$\underline{F}_l^{aero} = G_{22}\ddot{\underline{\kappa}}_l + G_{23}\ddot{\phi} + G_{25}\dot{\underline{\kappa}}_l + G_{26}\dot{\phi} + G_{21}1\underline{\lambda}_l + G_{213}\underline{\alpha}_l$$
$$\underline{M}_r^{aero} = H_{11}\ddot{\underline{\kappa}}_r + H_{13}\ddot{\phi} + H_{14}\dot{\underline{\kappa}}_r + H_{16}\dot{\phi} + H_{110}\underline{\lambda}_r + H_{112}\underline{\alpha}_r$$
$$\underline{M}_l^{aero} = H_{22}\ddot{\underline{\kappa}}_l + H_{23}\ddot{\phi} + H_{25}\dot{\underline{\kappa}}_l + H_{26}\dot{\phi} + H_{211}\underline{\lambda}_l + H_{213}\underline{\alpha}_l$$

where $\underline{\lambda}$ and $\underline{\alpha}$ are the inflow and angle of attack vectors defined at the coordinates, $\underline{s}_p$. $\underline{F}_r^{aero}$, $\underline{M}_r^{aero}$, $\underline{F}_l^{aero}$, and $\underline{M}_l^{aero}$ are vectors of aerodynamic forces and moments on the right and left wings, respectively. The method can be extended to include dynamic stall effects using the ONERA approach.

Aeroelastic Model

By combining the aerodynamic forces with the structure model, the full set of equations describing the aeroelastic motion is constructed,

$$\left[\begin{array}{c|c|c} Mt_{11} & 0 & Mt_{13} \\ \hline 0 & Mt_{22} & Mt_{23} \\ \hline Mt_{31} & Mt_{32} & Mt_{33} \end{array}\right] \begin{bmatrix} \ddot{\underline{\kappa}}_r \\ \ddot{\underline{\kappa}}_l \\ \ddot{\phi} \end{bmatrix} + \left[\begin{array}{c|c|c} Ct_{11} & 0 & Ct_{13} \\ \hline 0 & Ct_{22} & Ct_{23} \\ \hline Ct_{31} & Ct_{32} & Ct_{33} \end{array}\right] \begin{bmatrix} \dot{\underline{\kappa}}_r \\ \dot{\underline{\kappa}}_l \\ \dot{\phi} \end{bmatrix} + \left[\begin{array}{c|c|c} Kt_{11} & 0 & 0 \\ \hline 0 & Kt_{22} & 0 \\ \hline Kt_{31} & Kt_{32} & Kt_{33} \end{array}\right] \begin{bmatrix} \delta\underline{\kappa}_r \\ \delta\underline{\kappa}_l \\ \phi \end{bmatrix} + \left[\begin{array}{c|c} D_{11} & 0 \\ \hline 0 & D_{22} \\ \hline D_{31} & D_{32} \end{array}\right] \begin{bmatrix} \underline{\lambda}_r \\ \underline{\lambda}_l \end{bmatrix} = \begin{bmatrix} \underline{F}_1 \\ \underline{F}_2 \\ \underline{F}_3 \end{bmatrix}$$

$$\begin{bmatrix} \dot{\underline{\lambda}}_r \\ \dot{\underline{\lambda}}_l \end{bmatrix} = \left[\begin{array}{c|c|c} F_{11} & 0 & F_{13} \\ \hline 0 & F_{22} & F_{23} \end{array}\right] \begin{bmatrix} \ddot{\underline{\kappa}}_r \\ \ddot{\underline{\kappa}}_l \\ \ddot{\phi} \end{bmatrix} + \left[\begin{array}{c|c|c} F_{14} & 0 & F_{16} \\ \hline 0 & F_{25} & F_{26} \end{array}\right] \begin{bmatrix} \dot{\underline{\kappa}}_r \\ \dot{\underline{\kappa}}_l \\ \dot{\phi} \end{bmatrix} + \left[\begin{array}{c|c} F_{17} & 0 \\ \hline 0 & F_{18} \end{array}\right] \begin{bmatrix} \underline{\lambda}_r \\ \underline{\lambda}_l \end{bmatrix}$$

$$\begin{bmatrix} \underline{F}_1 \\ \underline{F}_2 \\ \underline{F}_3 \end{bmatrix} = \begin{bmatrix} B_{11} & 0 \\ 0 & B_{22} \\ 0 & 0 \end{bmatrix} \begin{bmatrix} \underline{v}_r \\ \underline{v}_l \end{bmatrix} + \begin{bmatrix} B_{111} & 0 \\ 0 & B_{212} \\ 0 & 0 \end{bmatrix} \begin{bmatrix} \delta\underline{\kappa}_{r,0} \\ \delta\underline{\kappa}_{l,0} \end{bmatrix} + \begin{bmatrix} B_{113} & 0 \\ 0 & B_{214} \\ B_{313} & B_{314} \end{bmatrix} \begin{bmatrix} \underline{\alpha}_{r,0} \\ \underline{\alpha}_{l,0} \end{bmatrix} + \begin{bmatrix} B_{115} & 0 \\ 0 & B_{216} \\ B_{315} & B_{316} \end{bmatrix} \begin{bmatrix} \underline{u}_{g,r} \\ \underline{u}_{g,l} \end{bmatrix}$$

where $\delta\underline{\kappa}_0 = \underline{\kappa}_0 - \underline{\kappa}_l$, $\underline{\kappa}_0$ is the curvature vector of the linearized system, $\underline{\kappa}_l$ is the initial curvature vector of the wing, and $\delta\underline{\kappa}$ is the change in the curvature. $\underline{u}_g$ is the direction of gravity in the body reference frame. The system matrices depend on the current state and the flight condition and must be continuously updated.

Preliminary Numerical Study

The present study investigates the effects of the active ply angles on the static and dynamic behavior of a wind-tunnel size model of an active flexible wing. The analysis model is a NACA0014 airfoil with four (passive) plies (0°/90°) of E-glass running the full length of the chord on both the top and bottom wing surfaces. Also, two active

fiber composite (AFC) plies at $+\theta$ and $-\theta$ on each of the top and bottom surfaces, covering approximately 95% of the surface. The AFCs are used here as a realization of an anisotropic piezocomposite actuator. The angles of the passive plies are held constant. The wing has a 2m semi-span, with a root chord of 15 cm. The wing starts tapering linearly at 0.5 m from the root, reaching a tip chord of 10 cm. Actuating the $+\theta$ plies with positive voltage and the $-\theta$ plies with negative voltage produces twist. Bending actuation is achieved by applying positive voltage to the top plies and a negative voltage to the bottom plies.

Figure 2 shows the effectiveness of the actuators for producing twist as a function of AFC ply angle. A 2000 V twist input was applied. At 0° the actuators have no capability for producing twist, and the maximum effectiveness is shown to be at 45°.

The increase in twist capability comes at the expense of bending authority. The 0° plies are much more effective in producing bend deformation than the 45° plies. As seen in Figure 3, which plots the maximum bending curvature for ply angles from 0° to 50°, the 0° plies produce more than three times the curvature as the 45°plies.

Variations in active ply angle that benefit twist authority may have an adverse effect on the static deflection due to aerodynamic loading, which in turn has an effect on the natural frequencies. Note that the natural frequencies of the wing do not only depend on the mass and stiffness distribution, but also on the steady deformed shape due to aerodynamic loading. When the wing is bent, the first torsion and first chordwise bending modes tend to coalesce into a "rocking" mode. This behavior cannot be captured using a linear model, linearized about the undeformed state.

As seen in Figure 4, which plots the wing tip displacement for flight speed U = 25 m/s as the angle of the active plies is varied from 0° to 45° the tip displacement increases by 22%.

Figure 5 plots the movement of the first four natural frequencies with respect to the active ply angle. For each angle, the wing was brought to its steady deformed shape at U = 30 m/s, and then the natural frequencies were obtained. Figure 6 shows the reduction in flutter speed as the active ply angle is varied.

Those simple results exemplify the capabilities of the proposed analysis and showed that the choice of actuation layup variables has a *profound* effect on the aeroelastic behavior of active conformable wings. By investigating only changes in the actuation ply angles, it was shown that adjustments to improve the twist authority of the active plies may lead to a deterioration in aeroelastic performance for reasons that are difficult for the designer to understand without iterative data.

A reduction in open loop flutter speed due to increasing the active ply angles to 45° may be recovered when active control is employed, so the closed loop response of the wing, as well as static performance, must be the measure of the merit of a particular wing structure.

References

[1] Ortega-Morales, M. and Cesnik, C. E. S., "Modeling and Control of the Aeroelastic Response of Highly Flexible Active Wings," AMSL Report #2000-2, 2000.

[2] Cesnik, C. E. S., Hodges, D. H., and Patil, M. J. "Aeroelasticity Analysis of Composite Wings," *37th Structures, Structural Dynamics, and Material Conference*, Salt Lake City, Utah, April 15—17, 1996, AIAA-96-1444-CP, pp. 1113—1123.

[3] Cesnik, C. E. S. and Shin, S.-J., "On the Modeling of Active Helicopter Blades," Int. Journal of Solids and Structures, Vol. 38, Nos. 10-13, March 2001, pp. 1765-1789.

[4] Patil, M. J., Hodges, D. H., and Cesnik, C. E. S., "Nonlinear Aeroelasticity and Flight Dynamics of High-Altitude Long-Endurance Aircraft," J. of Aircraft, Vol. 38, No. 1, January-February 2001, pp. 95–103.

[5] Peters, D. A. and Johnson, M. J., "Finite-State Airloads for Deformable Airfoils on Fixed and Rotating Wings", In *Symposium on Aeroelsasticity and Fluid/Structure Interaction, Proceedings of the Winter Annual Meeting.* ASME, November 6 -11, 1994.

[6] Peters, D. A., Karunamoorthy, S., and Cao, W. M., "Finite State Induced Flow Models; Part I: Two-Dimensional Thin Airfoil", *Journal of Aircraft*, Vol. 32, No. 2, March – April 1995.

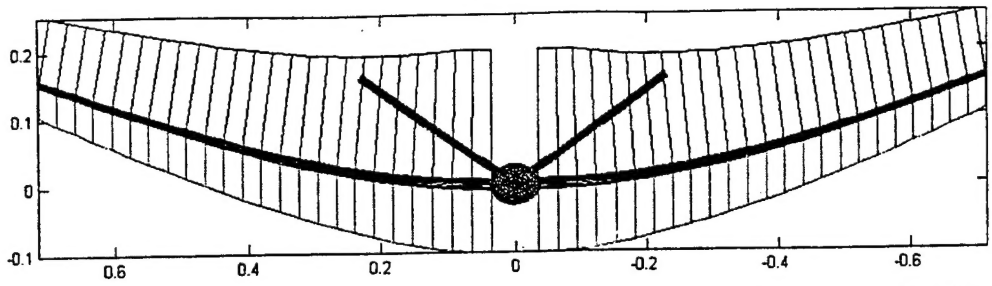

Figure 1: Two-wing roll model showing gravity and aerodynamic loading distributions

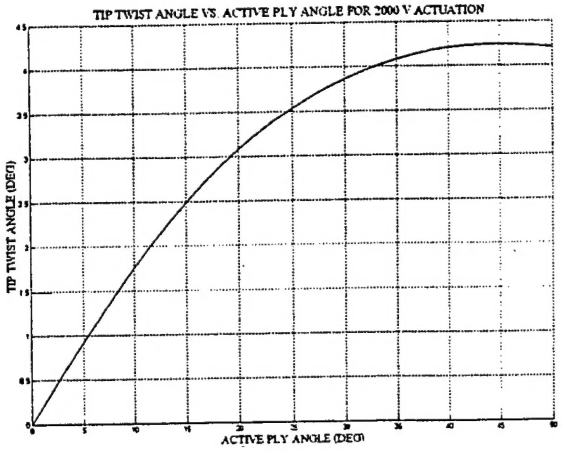

Figure 2: Changing in tip twist angle amplitude for different actuator ply angle in the active wing (2000 V input)

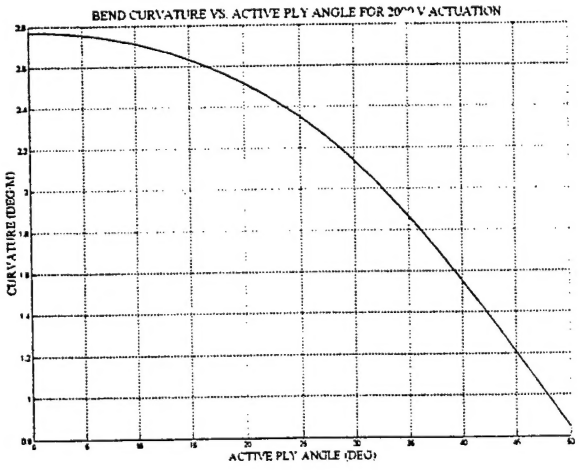

Figure 3: Changing in maximum bending curvature for different actuator ply angle in the active wing (2000 V input)

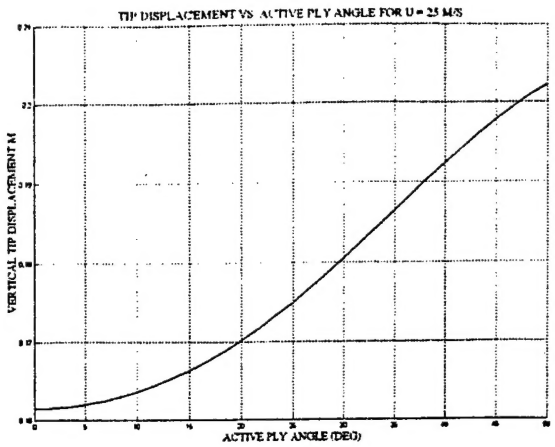

Figure 4: Changing in vertical tip displacement for different actuator ply angle in the active wing (U=25 m/s)

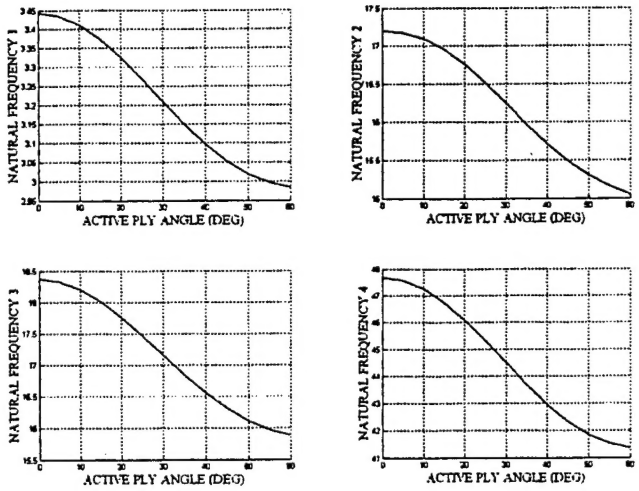

Figure 5: Variation in the natural frequencies of the active wing due to changing in the actuator ply angle

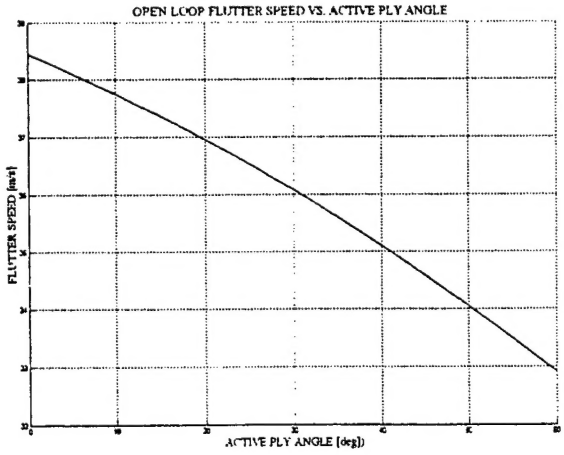

Figure 6: Reduction on the linearized flutter speed of the active wing due to changing in the actuator ply angle

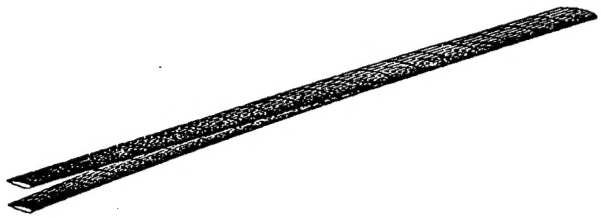

Figure 7: Wing deformation due to 2000 V bending actuation (figure compares deformed and undeformed states)

Principal Investigator Annual Data Collection (PIADC) Form

NOTE: If there is insufficient space on this survey to meet your data submissions, please submit additional data in the same format as identified below. ***The reporting period is September 1 through August 31 of the calendar year in which the report is given.***

PI DATA

Name (Last, First, MI): _Cesnik, Carlos E. S._____

Institution: __Massachusetts Institute of Technology_____

Contract/Grant No.: _F49620-01-1-0133_____

AFOSR USE ONLY
Project/Subarea: _____
NX: _____
FY: _____

NUMBER OF GRANT/CONTRACT CO-INVESTIGATORS

Faculty: ___1_____ Post-doctorates: __0_____ Graduate Students __1_____ Other:__0____

PUBLICATIONS RELATED TO AFOSR MENTIONED GRANT/CONTRACT

NOTE: List names in the following format: Last Name, First Name, MI

Include: Articles in peer reviewed publications, journals, book chapters and editorships of books

Do Not Include: Unreviewed proceedings, reports and abstracts; "Scientific American" type articles or articles that are not primary reports of research; articles submitted or accepted for publication but with a publication date outside the reporting period; articles "in preparation".

Name of journal, book, etc.: _____N/A_____

Title of Article: _____

Author(s): _____

Publisher (if applicable): _____

Volume: _____ Pages_____ Month : _____Year: _____

HONORS/AWARDS RECEIVED DURING CONTRACT/GRANT LIFETIME

Include: All honors and awards received during the lifetime of the contract or grant and any life achievement honors, such as Nobel prize, honorary doctorates, and society fc1lowships prior to this contract or grant.

Do Not Include: Honors and awards unrelated to the scientific field covered by the contract/grant

Honor/Award: __N/A_____ Year received: _____

Honor/Award Recipient: _____

Awarding Organization: _____

(Add additional pages as necessary)